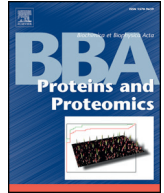




Contents lists available at ScienceDirect

Biochimica et Biophysica Acta

journal homepage: [www.elsevier.com/locate/bbapap](http://www.elsevier.com/locate/bbapap)

## Q1 Structural and nanomechanical comparison of epitaxially and 2 solution-grown amyloid $\beta$ 25–35 fibrils

Q2 Ünye Murvai <sup>a</sup>, Judit Somkuti <sup>a</sup>, László Smeller <sup>a</sup>, Botond Penke <sup>b</sup>, Miklós S.Z. Kellermayer <sup>a,c,\*</sup>

4 <sup>a</sup> Department of Biophysics and Radiation Biology, Semmelweis University, Tűzoltó u. 37-47, Budapest H-1094 Hungary

5 <sup>b</sup> Supramolecular and Nanostructured Materials Research Group of the Hungarian Academy of Sciences, Szeged, Dóm tér 8H-6720, Hungary

6 <sup>c</sup> MTA-SE Molecular Biophysics Research Group, Semmelweis University, Tűzoltó u. 37-47, Budapest, Szeged, Dóm tér 81094 Hungary

### 7 A R T I C L E I N F O

8 *Article history:*  
9 Received 29 July 2014  
10 Received in revised form 28 December 2014  
11 Accepted 11 January 2015  
12 Available online xxxxx

13 *Keywords:*  
14 Amyloid  
15 Atomic force microscopy  
16 Force spectroscopy  
17 Fourier transform infrared spectroscopy  
18  $\beta$ -Sheet structure  
19 Structural compaction

### A B S T R A C T

A $\beta$ 25–35, the fibril-forming, biologically active toxic fragment of the full-length amyloid  $\beta$ -peptide also forms fi- 20  
brils on mica by an epitaxial assembly mechanism. Here we investigated, by using atomic force microscopy, 21  
nanomechanical manipulation and FTIR spectroscopy, whether the epitaxially grown fibrils display structural 22  
and mechanical features similar to the ones evolving under equilibrium conditions in bulk solution. Unlike epi- 23  
taxially grown fibrils, solution-grown fibrils displayed a heterogeneous morphology and an apparently helical 24  
structure. While fibril assembly in solution occurred on a time scale of hours, it appeared within a few minutes 25  
on mica surface fibrils. Both types of fibrils showed a similar plateau-like nanomechanical response character- 26  
ized by the appearance of force staircases. The IR spectra of both fibril types contained an intense peak between 1620 27  
and 1640  $\text{cm}^{-1}$ , indicating that  $\beta$ -sheets dominate their structure. A shift in the amide I band towards greater 28  
wave numbers in epitaxially assembled fibrils suggests that their structure is less compact than that of 29  
solution-grown fibrils. Thus, equilibrium conditions are required for a full structural compaction. Epitaxial 30  
A $\beta$ 25–35 fibril assembly, while significantly accelerated, may trap the fibrils in less compact configurations. Con- 31  
sidering that under *in vivo* conditions the assembly of amyloid fibrils is influenced by the presence of extracellular 32  
matrix components, the ultimate fibril structure is likely to be influenced by the features of underlying matrix 33  
elements. 34

© 2015 Published by Elsevier B.V.

### 40 1. Introduction

41 Amyloid fibrils are nanoscale proteinaceous filaments that become  
42 deposited, in the form of plaques, in the extracellular space of different  
43 tissues in various degenerative disorders [1–3]. The main constituent of  
44 amyloid plaques in the brains of patients with Alzheimer's disease are  
45 amyloid beta (A $\beta$ ) fibrils composed of 39- to 43-residue-long A $\beta$  pep-  
46 tides, which are proteolytic by-products of the transmembrane amyloid  
47 precursor protein (APP) [4]. The undecapeptide A $\beta$ 25–35 is a naturally  
48 occurring proteolytic product of the full-length A $\beta$  [5,6]. It has been pro-  
49 posed that A $\beta$ 25–35 represents the biologically active region of A $\beta$  be-  
50 cause it is the shortest fragment that exhibits  $\beta$ -sheet-containing  
51 aggregated structures and retains the toxicity of the full-length peptide  
52 [7]. The peptide, which has a net charge of + 1, contains four polar res-  
53 idues at its N-terminus and seven predominantly hydrophobic residues

at its C-terminus [8]. The basic features of the A $\beta$ 25–35 fibril are similar 54  
to those formed from other A $\beta$  peptides. Accordingly,  $\beta$ -strands in an 55  
orientation perpendicular to the fibril axis connect to each other via hy- 56  
drogen bonds and line up to form  $\beta$ -sheet ribbons. The fibril contains 57  
several  $\beta$ -sheets that associate *via* amino acid side-chain packing to 58  
form the final protofilament structure [9]. 59

A $\beta$ 25–35 peptides incubated *in vitro* for an extended period of time 60  
(hours to days) form mature amyloid fibrils which are often used as an 61  
amyloid model. We have recently shown that the growth of A $\beta$ 25–35 62  
amyloid fibrils can be greatly facilitated by an epitaxial mechanism on 63  
mica surface. Under these conditions, the peptides form oriented fibril- 64  
lar network on mica surface within a few minutes [10–12]. Although it 65  
has been hypothesized that the epitaxially grown fibrils are identical 66  
to the ones evolving under equilibrium conditions in solution, a detailed 67  
structural comparison has not yet been carried out. Addressing the 68  
structure of epitaxially grown fibrils is compromised by the fact that 69  
only a fibrillar monolayer is available for investigation. In the present 70  
work we used atomic force microscopy, nanomechanics and FTIR spec- 71  
troscopy in total internal reflection mode for the structural comparison 72  
of A $\beta$ 25–35 fibrils grown epitaxially or in bulk solution. We find that al- 73  
though both fibril types are dominated by  $\beta$ -sheet structural elements 74

Abbreviations: AFM, atomic force microscopy; PBS, phosphate-buffered saline; FTIR, Fourier transform infrared

\* Corresponding author at: Department of Biophysics and Radiation Biology, Semmelweis University, Tűzoltó u. 37-47, Budapest H-1094, Hungary.

E-mail address: [kellermayer.miklos@med.semmelweis-univ.hu](mailto:kellermayer.miklos@med.semmelweis-univ.hu) (M.S.Z. Kellermayer).

<http://dx.doi.org/10.1016/j.bbapap.2015.01.003>  
1570-9639/© 2015 Published by Elsevier B.V.

Please cite this article as: Ü. Murvai, et al., Structural and nanomechanical comparison of epitaxially and solution-grown amyloid  $\beta$ 25–35 fibrils, Biochim. Biophys. Acta (2015), <http://dx.doi.org/10.1016/j.bbapap.2015.01.003>

that display similar nanomechanical properties, the fibrils grown in solution have more compact and polymorphic structure.

## 2. Materials and methods

### 2.1. Sample preparation

A $\beta$ 25–35 ( $^+H_3N-GSNKGAIIGLM-COO^-$ ) was produced by solid-state synthesis as published earlier [13]. For the study of epitaxially grown fibrils, the peptides were dissolved in dimethyl sulfoxide (DMSO) and transferred to Na-phosphate-buffered saline (Na-PBS) buffer (10 mM Na-phosphate, pH 7.4, 140 mM NaCl, 0.02% NaN<sub>3</sub>) at a final concentration of 0.5–1 mg/ml. Insoluble aggregates (“seeds”) were removed by centrifugation at 250,000 g and 4 °C for 2 h (Beckman Coulter OptimaTM MAX Ultracentrifuge). The supernatant was diluted to appropriate concentrations prior to further use. According to AFM analysis, the amount of remaining amorphous aggregates was <0.1%. In case of fibrils grown in solution, 0.5–1 mg peptide was dissolved in 10  $\mu$ l DMSO solution and further diluted with Na-PBS buffer to a final concentration of 0.5–1 mg/ml. The A $\beta$ 25–35 fibrils were grown in solution at room temperature for several (typically 2–10) days. The sample was then diluted prior to further investigations. In the case of FTIR experiments, 1 mg/ml A $\beta$ 25–35 fibril suspension was concentrated to 25 mg/ml by first vacuum drying in a SpeedVac instrument followed by dissolution of the pellet in D<sub>2</sub>O. Two microliters of 25 mg/ml A $\beta$ 25–35 samples was used for each measurement. Peptide concentration was measured with the quantitative bicinchoninic acid assay [14].

### 2.2. Atomic force microscopy

AFM was carried out by steps described in our previous publications [10–12,15–17]. Typically, 100  $\mu$ l samples were applied to a freshly cleaved mica surface. We used high-grade mica sheets (V2 grade,

#52–6, Ted Pella, Inc., Redding, CA). For the study of epitaxially grown fibrils, the seedless sample was incubated for 10 min on the mica surface. In case of fibrils grown in solution, 100  $\mu$ l of the several-day-old fibrils was pipetted onto freshly cleaved mica surface and then incubated for 30 min. After washing the surface with buffer to remove the unbound fibrils, we scanned the surface with AFM. The samples were imaged with AFM in buffer or in air. Non-contact mode AFM images were acquired with an Asylum Research MFP3D instrument (Santa Barbara, CA) using silicon-nitride cantilevers (Olympus BioLever, resonance frequency in air ~ 9 kHz; Olympus AC160 cantilever, resonance frequency in air ~ 330 kHz;). The 512  $\times$  512-pixel images were collected at a typical line-scanning frequency of 0.6–1.5 Hz and with a set point of 0.5–0.8 V.

### 2.3. Force measurements

Force spectroscopy on A $\beta$ 25–35 fibrils was carried out by established protocols [11,12,15–17]. Briefly, a 100  $\mu$ l sample of A $\beta$ 25–35 (8  $\mu$ M and 950  $\mu$ M for epitaxially and solution-grown fibrils, respectively) was pipetted on freshly cleaved mica and incubated for 10 min at room temperature. Unbound fibrils were removed by washing gently with buffer (Na-PBS). Surface-bound fibrils were mechanically manipulated by first pressing the cantilever (Olympus BioLever, lever A) tip against the surface, then pulling the cantilever away with a constant, pre-adjusted rate. Typical stretch rate was 500 nm/s. Experiments were carried out under aqueous buffer conditions (Na-PBS buffer, pH 7.4). Stiffness was determined for each cantilever by using the thermal method [18].

### 2.4. FTIR spectroscopy

The Fourier transform infrared (FTIR) spectra of amyloid fibrils growing in solution were investigated in a diamond anvil cell (Diacell,

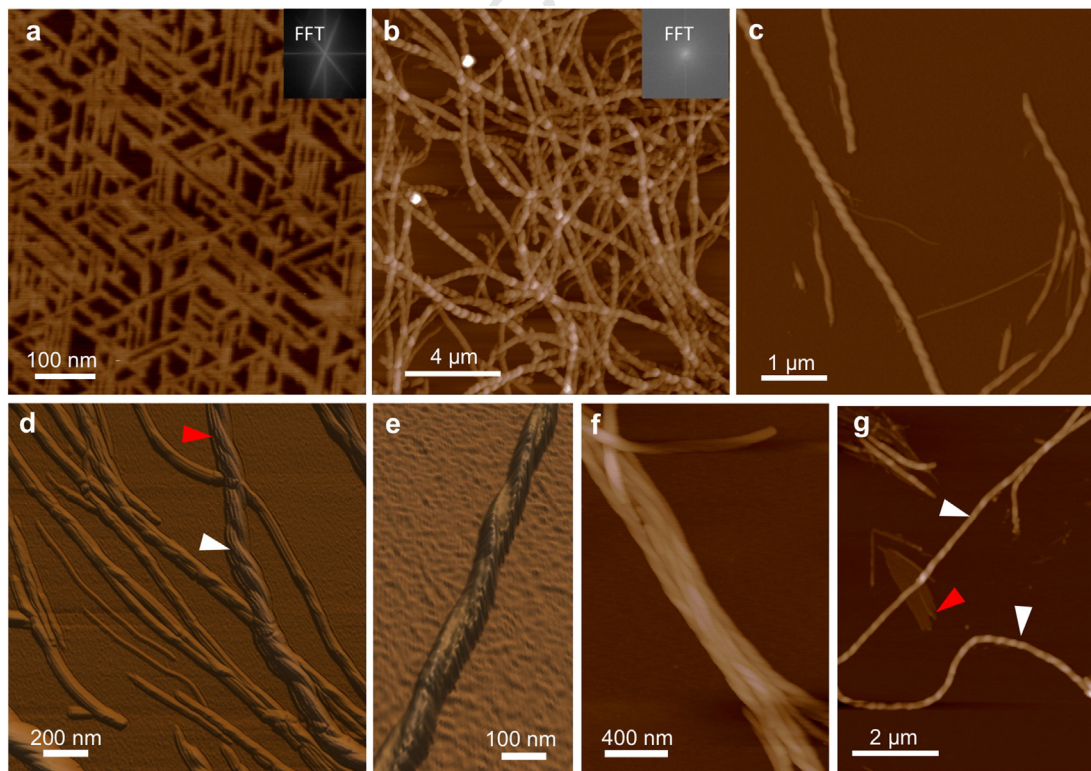


**Fig. 1.** AFM images showing the morphological appearance of A $\beta$ 25–35 fibrils. (a) Epitaxially grown, oriented A $\beta$ 25–35 fibril network on mica surface. (b–g) Mature A $\beta$ 25–35 fibrils assembled in solution and adsorbed subsequently onto mica. Fibrils display structural polymorphism and different levels of organizational hierarchy: (b) beaded appearance, (c) left-handed helix, (d) fibrils with apparent twist (white arrowhead) and striations (red arrowhead), (e) two fibrils twisted around each other, (f) bundle of twisted fibrils and (g) fibrils with left-handed twist (white arrowheads) and ones showing sheet-like appearance (red arrowhead). Insets, 2D-FFT of the respective AFM image.

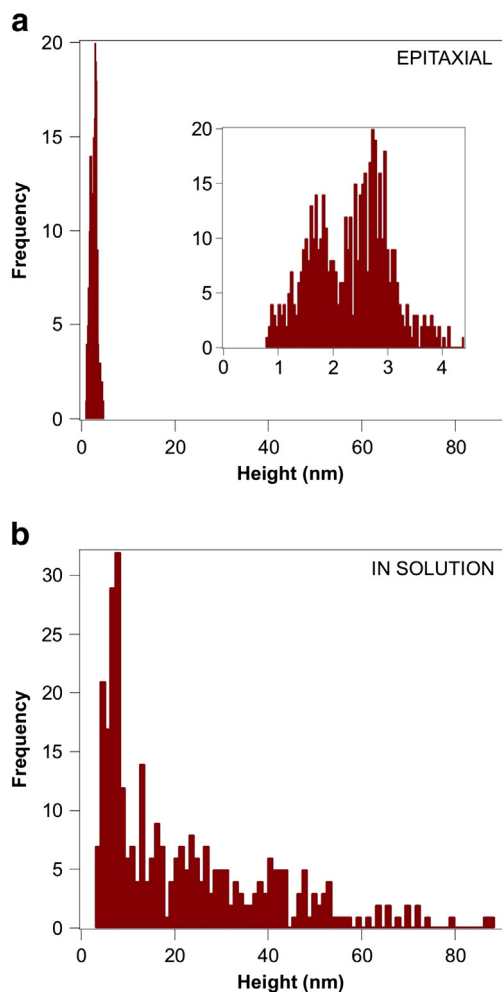


**Fig. 2.** Topographical height distribution of A $\beta$ 25–35 fibrils. (a) Distribution of topographical height of epitaxially grown A $\beta$ 25–35 fibrils. Inset shown the distribution within the range of 0–4.5 nm. (b) Distribution of topographical height of solution-grown A $\beta$ 25–35 fibrils.

132 Leicester, UK), which allowed the use of very small sample quantities.  
 133 To study the secondary structure of epitaxially grown fibrils, 100  $\mu$ l of  
 134 8  $\mu$ M seedless solution was incubated for 10 min on a freshly cleaved

sheet of mica. Unbound fibrils were removed by washing gently with 135  
 buffer, then the mica surface was dried in N<sub>2</sub> gas. Infrared spectra 136  
 were recorded by using a Bruker Vertex80v FTIR spectrometer equipped 137  
 with a high-sensitivity mercury cadmium telluride (MCT) detector. In 138  
 case of the anvil cell, a beam condenser (Bruker) was used to focus 139  
 the infrared light on the cell. Two hundred and fifty-six scans were col- 140  
 lected at 2 cm<sup>-1</sup> resolution. Spectral evaluation was performed by using 141  
 Opus (Bruker) software. The spectra of the mica experiments were 142  
 corrected for the interference fringes emerging on mica. 143

## 2.5. Image processing and data analysis 144

For data analysis, we used IgorPro v6.0 and ImageJ software. AFM 145  
 images and force spectra were analyzed with algorithms built in IgorPro 146  
 v6.03 MFP3D controller software (Wavemetrics, Lake Oswego, OR). 147

## 3. Results and discussion 148

### 3.1. Topographical structure of A $\beta$ 25–35 fibrils 149

To investigate the structure of A $\beta$ 25–35 fibrils and compare the fea- 150  
 tures of epitaxially grown and solution-grown fibrils, we collected topo- 151  
 graphical images with atomic force microscopy (AFM). Epitaxially 152  
 grown fibrils displayed a highly ordered trigonal arrangement on fresh- 153  
 ly cleaved mica surface within a few minutes of incubation (Fig. 1a). As 154  
 we have previously shown, the formation of oriented fibrils is the result 155  
 of epitaxial growth rather than the oriented binding of fibrils from solu- 156  
 tion. The negatively charged mica surface, in a manner similar to phos- 157  
 pholipid membranes [19], interacts with A $\beta$ 25–35 so that an apparently 158  
 cooperative interaction between the positively charged  $\epsilon$ -amino group 159  
 of Lys28 and the K<sup>+</sup>-binding pocket of the mica lattice determines the 160  
 oriented binding [10,11]. The trigonal orientation of epitaxially growing 161  
 A $\beta$ 25–35 fibrils is consistent with the hexagonal crystalline lattice struc- 162  
 ture of the exposed mica surface. The fibrils follow one of the three main 163  
 directions dictated by the hexagonal array of the surface lattice, al- 164  
 though it is not yet known which symmetry framework (i.e., axes cross- 165  
 ing the corners *versus* the sides of the hexagons) is preferred. Mica itself 166  
 lacks direct biological importance and significance. However, because 167  
 its negatively charged surface binding sites are arranged in a spatially 168  
 periodic manner (distance between consecutive K<sup>+</sup>-binding pockets is 169  
 5.2 Å) similarly to biological polymer systems such as collagen or 170  
 glucosaminoglycans [20–22], the mica-assisted growth of amyloid 171

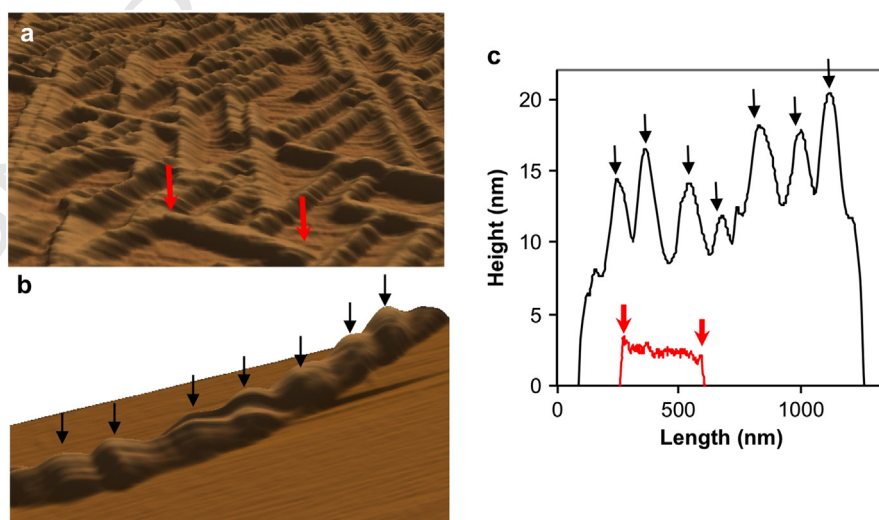


**Fig. 3.** Axial topography of A $\beta$ 25–35 fibrils. (a) AFM image of an epitaxially grown A $\beta$ 25–35 fibril selected for analysis, red arrows. (b) AFM image of a solution-grown A $\beta$ 25–35 fibril. Arrows highlight the axial periodic structures. (c) Local topographical height of fibrils along the axial contour. Black trace, solution-grown fibrils, red trace, epitaxially grown fibrils. Arrows correspond to the ones in the respective AFM images (a and b).



172 fibrils may provide clues to the mechanisms of *in vivo* fibrillogenesis fac-  
 173 cilitated by extracellular matrix components.

174 To explore the structure of solution-grown A $\beta$ 25–35 fibrils, an ali-  
 175 quot of fibrils incubated for several days was applied to mica. A poly-  
 176 morphic, structurally heterogeneous picture emerged (Fig. 1b–g).  
 177 Some of the fibrils displayed beaded (Fig. 1b) or sheet-like (Fig. 1g)  
 178 appearance, but most frequently a left-handed helical structure was  
 179 apparent (Fig. 1c–g). Interestingly, trigonally oriented fibrils were  
 180 completely absent, indicating that the free A $\beta$ 25–35 peptide concentra-  
 181 tion has, in these samples, already fallen below the critical concentra-  
 182 tion for epitaxial fibril formation. This observation supports the notion  
 183 that epitaxially and solution-grown fibrils indeed represent two distinct  
 184 populations of A $\beta$ 25–35 fibrils, which are segregated according to their

185 assembly mechanisms. That is, as long as monomeric A $\beta$ 25–35 peptide  
 186 species are present in large enough solution concentration, the proper-  
 187 ties of mica dictate the kinetics of fibril formations and the structure of  
 188 the emerging fibril. If, however, mature fibrils have already formed in  
 189 solution, the presence of mica does not appear to have a determinant ef-  
 190 fect on fibril structure. Therefore, the heterogenous ensemble of fibril  
 191 structures seen in our AFM images likely reflects the variety of equilib-  
 192 rium assembly pathways of A $\beta$ 25–35 fibril formation.

193 To quantitate the structural features of the fibrils, we measured their  
 194 topographical height distribution (Fig. 2). The range of topographical  
 195 height was 0.8–4 nm and 7–40 nm for epitaxially ( $n = 513$ ) and  
 196 solution-grown fibrils ( $n = 325$ ), respectively. As reported previously  
 197 for epitaxially grown fibrils, the structural unit with 0.8 nm height

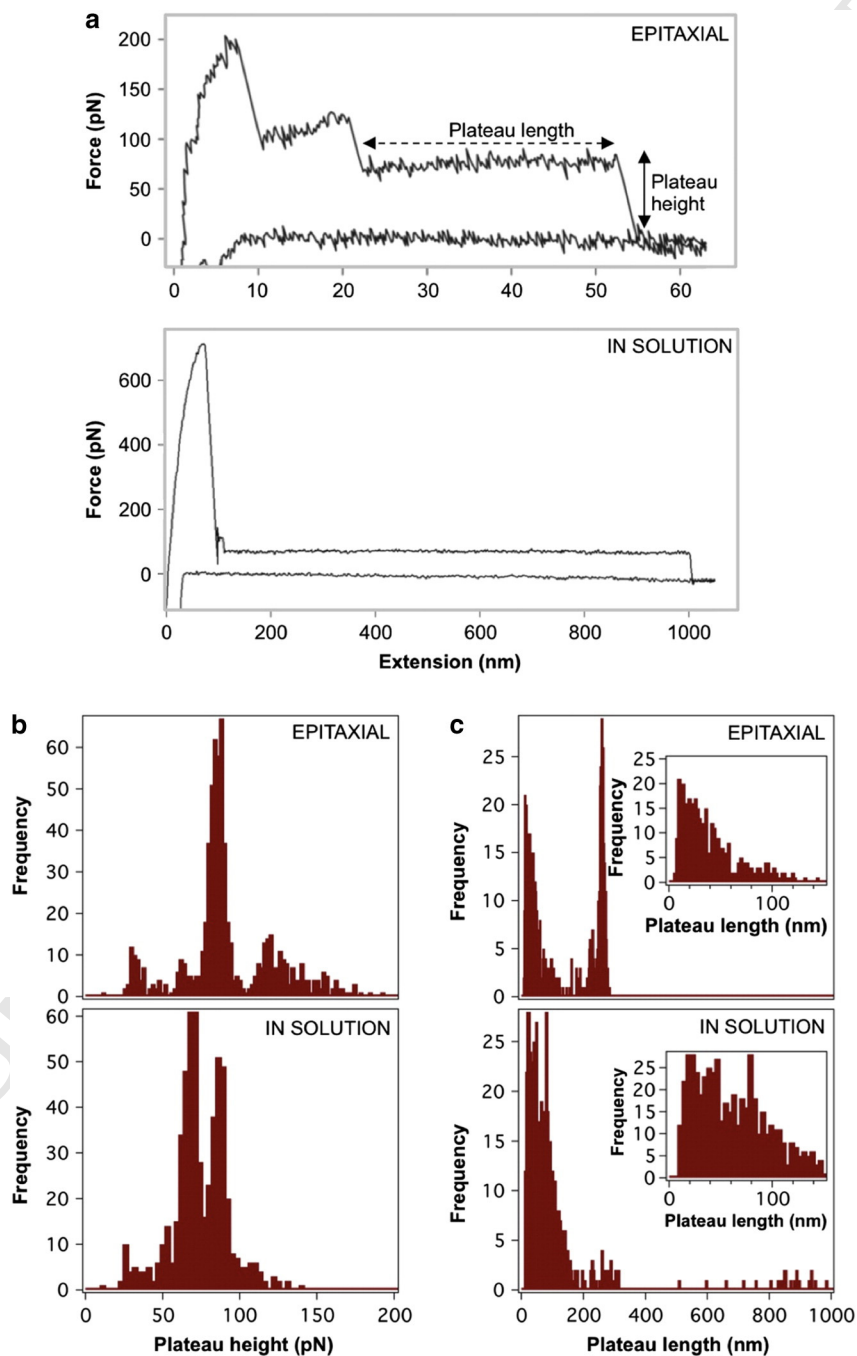


**Fig. 4.** Nanomechanics of A $\beta$ 25–35 fibrils. (a) Representative force curve for an epitaxially grown (top trace) and a solution-grown A $\beta$ 25–35 fibril (bottom trace). (b) Distribution of plateau height for epitaxially grown (top graph, number of data points 690) and solution-grown (bottom graph, number of data points 585) A $\beta$ 25–35 fibrils. (c) Distribution of plateau length for fibrils grown epitaxially (top graph) and in solution (bottom graph). Insets show the plateau length distributions within the range of 0–150 nm.

most likely corresponds to a single  $\beta$ -sheet [10]. Accordingly, one to five  $\beta$ -sheets build up one epitaxially grown fibril, whereas solution-grown fibrils may contain several tens of  $\beta$ -sheets in parallel.

Epitaxially grown fibrils were significantly shorter than solution-grown fibrils because their length is determined by steric constraints. Whenever the end of an epitaxially growing fibril reaches another fibril on the mica surface, its further growth is halted. Whereas the oriented, epitaxially grown fibrils were only 0.2–3  $\mu\text{m}$  long [10], the length of the fibrils formed in solution, which depends on the free monomer concentration, may reach 10–15  $\mu\text{m}$ .

To reveal further detail about the structural features, we measured the variation of height along the longitudinal axis of A $\beta$ 25–35 fibrils. The axial variation of the topographical height was low in the case of epitaxially grown fibrils (Fig. 3a) when compared with that of solution-grown fibrils (Fig. 3b). Solution-grown fibrils most often displayed distinct periodicity related to the underlying left-handed helical structure. The periodicity of these fibrils varied between 50 and 300 nm. Importantly, it took several hours for mature solution-grown fibrils with more-or-less consolidated structures to appear. By contrast, oriented, epitaxially grown fibrils merged within a few minutes after the application of sample onto the mica surface. The acceleration of fibrillogenesis kinetics indicates that mica serves as a catalyzer of A $\beta$ 25–35 formation. Within an *in vivo* environment that displays periodically arranged binding sites, such as collagen or glucosaminoglycans [20–22], a similarly catalyzed fibrillogenesis may also be feasible.

### 3.2. Nanomechanics of A $\beta$ 25–35 fibrils

Individual fibrils of either epitaxially or solution-grown A $\beta$ 25–35 were mechanically manipulated in order to characterize the intrafibrillar interactions. The nanomechanical behavior of A $\beta$ 25–35 fibrils is characterized by the appearance of force plateaus, which correspond to the force-driven unzipping of protofilaments (Fig. 4a) [15–17]. The height of the plateaus is related to the force necessary to unzip the component protofilaments from the underlying fibril driven by the mechanical rupture of the intrafibrillar (i.e., inter-protofilament) interactions (Fig. 4b). Therefore, plateau forces are related to the mechanical stability of the fibril [17]. The higher the plateau, the greater the force necessary to unzip protofilaments and *vice versa*. The length of the force plateau corresponds to the distance between consecutive protofilament rupture events (Fig. 4c). The longer the plateau, the longer it takes for the protofilament to rupture, along its length or at its attachment points, during mechanical unzipping [17]. Thus, plateau length may be loosely correlated with the length of the A $\beta$ 25–35 fibrils. The overall appearance

of the force spectra was similar for amyloid  $\beta$ 25–35 fibrils grown epitaxially or in solution. Both types of fibrils showed plateau-like nanomechanical responses pointing at a similar subfibrillar structure in which protofilaments line up in parallel to form bundles. The fundamental plateau force, defined as the force of the smallest mode within a multimodal distribution [17], was around 30 pN for the epitaxially ( $n = 690$ ) and solution-grown fibrils ( $n = 585$ ) (Fig. 4b). The multimodality of the plateau force histogram is attributed to a coupling between parallel protofilaments within the fibril. Qualitatively similar multimodality is reflected in the topographical height distribution of the fibrils (Fig. 2). Although the plateau length distribution was rather similar for the two fibril types, we sometimes observed very long plateaus in the case of solution-grown fibrils (up to 1000 nm long, Fig. 4c), which are likely due to the unzipping of the entire fibril from the substrate surface [23].

### 3.3. FTIR spectroscopy

The detailed structural features of the A $\beta$ 25–35 fibrils were further explored with Fourier transform infrared (FTIR) spectroscopy. FTIR spectroscopy is frequently used to detect the presence of  $\beta$ -sheet secondary structure and can be adapted for the unconventional arrangement of the surface-adsorbed epitaxially grown A $\beta$ 25–35 fibril sample. The approximate position of an IR absorption band is determined by the vibrating masses, the bond type (single, double or triple), the structural location of the electron withdrawing and donating effects of the intra- and intermolecular environment and by coupling with other vibrations [24]. Bands between 1600 and 1700  $\text{cm}^{-1}$  are assigned to amide I modes (essentially C = O stretching vibrations of the amide group) and are sensitive to protein secondary structure. As a rule of thumb, a peak near 1645  $\text{cm}^{-1}$  is indicative of random coil, 1655  $\text{cm}^{-1}$  of  $\alpha$ -helix and 1620–1640  $\text{cm}^{-1}$  of  $\beta$ -sheet [24–27].

To study the secondary structure of epitaxially grown fibrils, a seedless solution of A $\beta$ 25–35 peptides was incubated on a freshly cleaved sheet of mica, which was then investigated in total internal reflection mode. To measure the IR spectrum of solution-grown A $\beta$ 25–35 fibrils, a sample incubated for 14 days was used. The IR spectra of the epitaxially and solution-grown fibrils contained an intense peak at 1630 and 1623  $\text{cm}^{-1}$ , respectively (Fig. 5). Based on the spectral position of the dominant peak, we conclude that  $\beta$ -sheet elements dominate the structure of both fibril species. A smaller band at 1675  $\text{cm}^{-1}$  was also present. Consequently, both types of fibrils are likely to contain anti-parallel  $\beta$ -sheet structures. The assignment of an anti-parallel  $\beta$ -sheet is based on the observation of a peak near 1680  $\text{cm}^{-1}$  that arises due to transition dipole coupling and is absent in a parallel  $\beta$ -sheet [28].

Even though both fibril types have similar secondary structures, there are slight differences: the shift in the amide I band from 1623  $\text{cm}^{-1}$  in the solution-grown fibrils to 1630  $\text{cm}^{-1}$  in the epitaxially grown ones points at a reduced transition dipole coupling and weaker hydrogen bonds in the epitaxial fibrils. These spectral changes reflect the reduced structural compaction of the epitaxial fibrils compared to the ones grown in solution. Conceivably, the oriented arrangement of epitaxially grown fibrils, determined by the interaction between the Lys28 side chains and the K<sup>+</sup>-binding pockets of mica, places constraints on the subsequent binding of further A $\beta$ 25–35 peptides, thereby resulting in a loosened structure. Thus, while the overall features of epitaxially and solution-grown fibrils are almost identical, the smaller compaction of epitaxially evolved fibrils suggests that interactions with the underlying substrate alter fibril structure.

### 4. Conclusions

A $\beta$ 25–35 fibrils evolve not only in solution conditions but also in an accelerated manner, via epitaxial mechanism, on mica surface. In the present work, we tested whether the fibrils formed under equilibrium conditions are significantly different from those grown epitaxially on the surface. Whereas epitaxially grown fibrils have a uniform

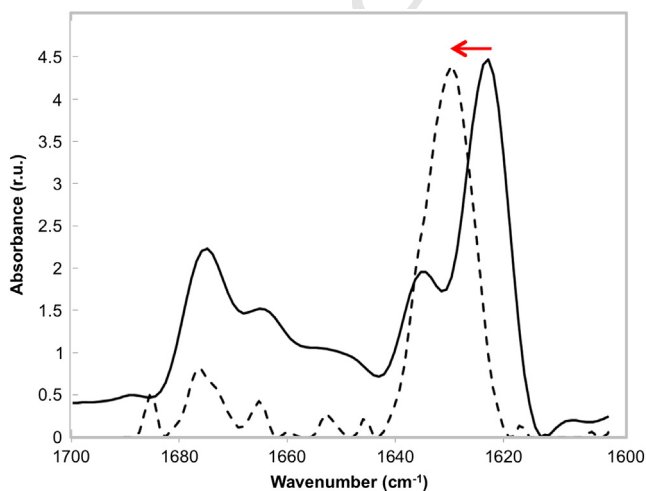


Fig. 5. Deconvoluted FTIR spectra of epitaxially (dashed line) and solution-grown (solid line) A $\beta$ 25–35 fibrils. Red arrow indicates the shift of the major peak towards greater wave numbers.

topographical structure characterized by straight fibrils and smooth surface, solution-grown fibrils display considerable polymorphism and structural heterogeneity, curved shape, left-handed helical structure and an axial periodicity ranging between 50 and 300 nm. FTIR spectroscopy revealed that the main structural feature of both fibril types is the  $\beta$ -sheet. Epitaxially grown fibrils are less compact, however, than the ones grown under equilibrium conditions in solution, suggesting that the underlying substrate surface may influence the final structure of the amyloid fibril.

### 311 Acknowledgements

312 This work was supported by grants from the Hungarian Science  
313 Foundation (OTKA K84133 and OTKA K109480). The research leading  
314 to these results has received funding from the European Union's  
315 Seventh Framework Program (FP7/2007-2013) under grant agreement  
316 no. HEALTH-F2-2011-278850 (INMIND).

### 317 References

- 318 [1] J. Hardy, D.J. Selkoe, The amyloid hypothesis of Alzheimer's disease: progress and  
319 problems on the road to therapeutics, *Science* 297 (2002) 353–356.  
320 [2] D.J. Selkoe, Alzheimer's disease: genes, proteins, and therapy, *Physiol. Rev.* 81  
321 (2001) 741–766.  
322 [3] L.C. Serpell, C.C. Blake, P.E. Fraser, Molecular structure of a fibrillar Alzheimer's A  
323 beta fragment, *Biochemistry* 39 (2000) 13269–13275.  
324 [4] D.J. Selkoe, Images in neuroscience. Alzheimer's disease: from genes to pathogenesis,  
325 *Am. J. Psychiatry* 154 (1997) 1198.  
326 [5] G. Forloni, R. Chiesa, S. Smiroldo, L. Verga, M. Salmona, F. Tagliavini, N. Angeretti,  
327 Apoptosis mediated neurotoxicity induced by chronic application of beta amyloid fragment  
328 25–35, *Neuroreport* 4 (1993) 523–526.  
329 [6] B.A. Yankner, L.K. Duffy, D.A. Kirschner, Neurotrophic and neurotoxic effects of amyloid  
330 beta protein: reversal by tachykinin neuropeptides, *Science* 250 (1990) 279–282.  
331 [7] C.J. Pike, A.J. Walencewicz-Wasserman, J. Kosmoski, D.H. Cribbs, C.G. Glabe, C.W.  
332 Cotman, Structure-activity analyses of beta-amyloid peptides: contributions of the  
333 beta 25–35 region to aggregation and neurotoxicity, *J. Neurochem.* 64 (1995)  
334 253–265.  
335 [8] M. van Veen, P. O'Shea, The interaction of the neurodegenerative fragment of the  
336 beta-amyloid peptide with phospholipid membranes, *Biochem. Soc. Trans.* 23  
337 (1995) 547S.  
338 [9] T.R. Jahn, O.S. Makin, K.L. Morris, K.E. Marshall, P. Tian, P. Sikorski, L.C. Serpell, The  
339 common architecture of cross-beta amyloid, *J. Mol. Biol.* (2009).  
340 [10] Á. Karsai, L. Grama, Ü. Murvai, K. Soós, B. Penke, M.S. Kellermayer, Potassium-  
341 dependent oriented growth of amyloid  $\beta$ 25–35 fibrils on mica, *Nanotechnology*  
342 18 (2007) 345102.  
343  
344  
345

- [11] A. Karsai, U. Murvai, K. Soos, B. Penke, M.S. Kellermayer, Oriented epitaxial growth  
of amyloid fibrils of the N27C mutant beta 25–35 peptide, *Eur. Biophys. J.* 37  
(2008) 1133–1137. 346  
[12] U. Murvai, K. Soos, B. Penke, M.S. Kellermayer, Effect of the beta-sheet-breaker pep-  
tide LPPFD on oriented network of amyloid beta25–35 fibrils, *J. Mol. Recognit.* 24  
(2011) 453–460. 347  
[13] M. Zarandi, K. Soos, L. Fulop, Z. Bozso, Z. Datki, G.K. Toth, B. Penke, Synthesis of Abeta  
[1–42] and its derivatives with improved efficiency, *J. Pept. Sci.* 13 (2007) 94–99. 350  
[14] P.K. Smith, R.I. Krohn, G.T. Hermanson, A.K. Mallia, F.H. Gartner, M.D. Provenzano,  
E.K. Fujimoto, N.M. Goeke, B.J. Olson, D.C. Klenk, Measurement of protein using  
bicinchoninic acid, *Anal. Biochem.* 150 (1985) 76–85. 352  
[15] A. Karsai, Z. Martonfalvi, A. Nagy, L. Grama, B. Penke, M.S. Kellermayer, Mechanical  
manipulation of Alzheimer's amyloid beta1–42 fibrils, *J. Struct. Biol.* 155 (2006)  
316–326. 355  
[16] A. Karsai, A. Nagy, A. Kengyel, Z. Martonfalvi, L. Grama, B. Penke, M.S. Kellermayer,  
Effect of lysine-28 side-chain acetylation on the nanomechanical behavior of  
alzheimer amyloid beta25–35 fibrils, *J. Chem. Inf. Model.* 45 (2005) 1641–1646. 358  
[17] M.S. Kellermayer, L. Grama, A. Karsai, A. Nagy, A. Kahn, Z.L. Datki, B. Penke, Revers-  
ible mechanical unzipping of amyloid beta-fibrils, *J. Biol. Chem.* 280 (2005)  
8464–8470. 361  
[18] J.L. Hutter, J. Bechhoefer, Calibration of atomic-force microscope tips, *Rev. Sci.* 364  
*Instrum.* 64 (1993) 1868–1873. 365  
[19] E. Terzi, G. Holzemann, J. Seelig, Alzheimer beta-amyloid peptide 25–35: electrostatic  
interactions with phospholipid membranes, *Biochemistry* 33 (1994) 7434–7441. 366  
[20] G. Esposito, A. Corazza, V. Bellotti, Pathological self-aggregation of beta(2)-micro-  
globulin: a challenge for protein biophysics, *Subcell. Biochem.* 65 (2012) 165–183. 367  
[21] A. Relini, C. Canale, S. De Stefano, R. Rolandi, S. Giorgetti, M. Stoppini, A. Rossi, F.  
Fogolari, A. Corazza, G. Esposito, A. Gliozzi, V. Bellotti, Collagen plays an active role  
in the aggregation of beta2-microglobulin under physiopathological conditions of  
dialysis-related amyloidosis, *J. Biol. Chem.* 281 (2006) 16521–16529. 372  
[22] A. Relini, S. De Stefano, S. Torrassa, O. Cavalleri, R. Rolandi, A. Gliozzi, S. Giorgetti, S.  
Raimondi, L. Marchese, L. Verga, A. Rossi, M. Stoppini, V. Bellotti, Heparin strongly  
enhances the formation of beta2-microglobulin amyloid fibrils in the presence of  
type I collagen, *J. Biol. Chem.* 283 (2008) 4912–4920. 375  
[23] Y.L. Lyubchenko, S. Sherman, L.S. Shlyakhtenko, V.N. Uversky, Nanoimaging for pro-  
tein misfolding and related diseases, *J. Cell. Biochem.* 99 (2006) 52–70. 377  
[24] A. Barth, Infrared spectroscopy of proteins, *Biochim. Biophys. Acta* 1767 (2007) 380  
1073–1101. 381  
[25] J.L. Arrondo, A. Muga, J. Castresana, F.M. Goni, Quantitative studies of the structure of  
proteins in solution by Fourier-transform infrared spectroscopy, *Prog. Biophys. Mol.*  
*Biol.* 59 (1993) 23–56. 382  
[26] Y.N. Chirgadze, B.V. Shestopalov, S.Y. Venyaminov, Intensities and other spectral pa-  
rameters of infrared amide bands of polypeptides in the beta- and random forms,  
*Biopolymers* 12 (1973) 1337–1351. 385  
[27] C.R. Middaugh, H. Mach, J.A. Ryan, G. Sanyal, D.B. Volkin, Infrared spectroscopy,  
*Methods Mol. Biol.* 40 (1995) 137–156. 386  
[28] W.H. Moore, S. Krimm, Transition dipole coupling in amide I modes of  
betapolypeptides, *Proc. Natl. Acad. Sci. U. S. A.* 72 (1975) 4933–4935. 387  
388  
389  
390  
391